



# Pressure tuning of thermoelectric performance in FeNbSb

HPSTAR  
814-2019



Hong-Jie Pang<sup>a</sup>, Hao Yu<sup>a</sup>, Liu-Cheng Chen<sup>a</sup>, Chen-Guang Fu<sup>b, c</sup>, Tie-Jun Zhu<sup>b</sup>,  
Xiao-Jia Chen<sup>a, \*</sup>

<sup>a</sup> Center for High Pressure Science and Technology Advanced Research, Shanghai, 201203, China

<sup>b</sup> State Key Laboratory of Silicon Materials, School of Materials Science and Engineering, Zhejiang University, Hangzhou, 310027, China

<sup>c</sup> Max Planck Institute for Chemical Physics of Solids, Dresden, 01187, Germany

## ARTICLE INFO

### Article history:

Received 31 May 2019

Received in revised form

4 July 2019

Accepted 15 July 2019

Available online 19 July 2019

### Keywords:

thermoelectricity

High pressure

Raman spectroscopy

Transport properties

## ABSTRACTS

Thermoelectric materials offer an ideal solution for the global energy crisis and environmental pollution as which can directly convert waste heat into electricity. From the view of device application, achieving large figure of merit  $zT$  at room temperature is highly desirable. Here, we choose a half-Heusler compound  $\text{FeNb}_{0.8}\text{Ti}_{0.2}\text{Sb}$  with a maximum  $zT$  of 1.1 at 1100 K as an example. By using the developed techniques for the high-pressure measurements, we investigate the potential of pressure to tune the thermoelectric performance at room temperature. An obvious improvement of  $zT$  by about 62.5 % is achieved at 4 GPa. A pressure-induced electronic topological transition is proposed to contribute to such an improvement. This study points to a promising avenue to enhance the  $zT$  of half-Heusler compounds.

© 2019 Elsevier B.V. All rights reserved.

## 1. Introduction

Energy shortage and environmental pollution are two major global problems. Seeking alternative clean energy with sustainable development has become one of the main themes around the world. Thermoelectric materials could directly convert waste heat into clean energy without additional pollution and hence is an excellent candidate to the global sustainable energy solution [1–4]. The potential applications need thermoelectric materials with high conversion efficiency, especially for the applications at room temperature. However, achieving high conversion efficiency is difficult. The conversion efficiency of a thermoelectric material is determined by a dimensionless figure of merit [5]  $zT = S^2\sigma\kappa^{-1}T$ , where  $S$ ,  $\sigma$ ,  $\kappa$ , and  $T$  are the Seebeck coefficient, electrical conductivity, thermal conductivity, and absolute temperature, respectively. The parameters are independent and difficult to be optimized. Nowadays many strategies are used to obtain efficient thermoelectric materials. One effective strategy is to explore new promising materials with desired thermoelectric performance [6–10]. The other strategy is to optimize the electrical transport properties or to reduce the thermal conductivity, such as doping [11], mesostructure [12] and alloying [13].

Compared with doping, mesostructure and alloying, pressure is recognized as a clean and more effective way to tune the electronic and lattice structure. The application of pressure has led to large improvement of the electrical transport properties in many thermoelectric materials, such as  $\text{CuInTe}_2$  [14], palladium sulfide [15],  $\text{Sr}_3\text{Ga}_{16}\text{Ge}_{30}$  [16] and  $\text{Bi}_2\text{Te}_3$  [17]. Therefore, the maximum  $zT$  value at high temperature in a material can be expected at room temperature by applying pressure. In recent years, half-Heusler materials have received a great deal of interest due to their typically large Seebeck coefficient and good electrical conductivity [18–25]. Extensive studies have shown that the remarkable electrical properties result from the narrow band gap [26–31]. However, the relatively high thermal conductivity limit the usage of half-Heuslers as ideal thermoelectric materials [32]. FeNbSb-based half-Heusler compounds have been recognized to exhibit an outstanding thermoelectric performance. The thermal conductivity of FeNbSb is largely reduced for 20% Ti doped sample compared with the pure FeNbSb [33]. The disorder [34,35] and mode Grüneisen parameters [36] have been reported to provide clues for the reduced thermal conductivity. As a result, the maximum  $zT$  is 1.1 around 1100 K [33]. As the representative of half-Heusler materials, whether the maximum  $zT$  value can be obtained at room temperature by applying pressure is unknown due to the experimental difficulties. Moreover, disorder is complicated in this system that it is difficult to be explained clearly by computation.

\* Corresponding author.

E-mail address: [xjchen@hpstar.ac.cn](mailto:xjchen@hpstar.ac.cn) (X.-J. Chen).

In this work, we choose  $\text{FeNb}_{0.8}\text{Ti}_{0.2}\text{Sb}$  as an example to show how pressure tune the thermoelectric properties. The Seebeck coefficient, electrical resistivity are measured up to 20 GPa. The pressure-dependent thermal conductivity were estimated. And the pressure-dependent  $zT$  values were obtained. By means of pressure, we find that the thermoelectric transport properties of the room-temperature  $\text{FeNb}_{0.8}\text{Ti}_{0.2}\text{Sb}$  are improved in the studied pressure range. Pressure is proven to be an avenue for such an improvement. Moreover, an electronic topological transition (ETT) is observed at low pressure. Such an ETT effect is proposed to contribute to the anomalies of electrical transport properties in the sample. Furthermore, the potential of pressure to tune the thermoelectric properties in half-Heusler compound will be exploited.

## 2. Experimental details

The sample ingot with a nominal composition of  $\text{FeNb}_{0.8}\text{Ti}_{0.2}\text{Sb}$  used in the experiment was synthesized by levitation melting. The obtained ingot was mechanically milled to obtain fine-grained powders. Afterwards, the powders were immediately impacted by spark plasma sintering at 1123 K for 10 min under 65 MPa (megapascal). Further experimental details are given previously [33]. The as-sintered samples were annealed at 1123 K for 8 days. The pressure was carried out with various types of diamond anvil cells and determined by the standard ruby fluorescent technique up to about 20 GPa [37]. The Seebeck coefficient measurements as a function of pressure were made in symmetry diamond anvil cell at ambient temperature. The pressure dependent resistivity measurements were performed by using a nonmagnetic diamond anvil cell made of Be–Cu alloy in Physical Property Measurement System (Quantum Design). The Hall coefficient measurements under pressure were also completed using a Physical Property Measurement System (Quantum Design). The pressure dependence of Raman spectra were measured using a symmetry diamond anvil cell. The incident light was emitted by a Sapphire laser (Coherent) with excitation laser wavelength of 532 nm. The scattered light was focused on an 1800 g/mm grating and analyzed by a Princeton Instrument spectrometer coupled to a CCD detector. The details have been described previously [36].

## 3. Results and discussion

Fig. 1(a) and (b) show the temperature dependence of  $zT$  at ambient pressure [34] and the pressure dependence of  $zT$  at 300 K, respectively. The  $\text{FeNb}_{0.8}\text{Ti}_{0.2}\text{Sb}$  has the crystal structure of half-Heusler compounds (as shown in the inset of Fig. 1 (a)). With increasing temperature, the  $zT$  increases rapidly and exhibits a maximum of 1.1 at 1100 K. The  $zT$  at 300 K is 0.08. The red dotted line represents guides to the eye. As observed, the  $zT$  exhibits a nonmonotonic behavior and a maximum 0.13 around 4 GPa. The maximum  $zT$  value of room-temperature  $\text{FeNb}_{0.8}\text{Ti}_{0.2}\text{Sb}$  under pressure has increased by 62.5%. The pressure effects on the improvement of the thermoelectric performance are illustrated below.

The pressure-dependent Seebeck coefficient was measured by the technique developed recently [14,15]. Based on the definition of the Seebeck coefficient  $S = \Delta V/\Delta T$ , we measure the thermoelectric voltages and temperature gradients of the sample at various pressures. The Seebeck coefficient values are obtained by the linear fitting of the data. The representative data are shown at the left panel of Fig. 2. The designed diagram for Seebeck coefficient measurement under pressure is illustrated in the inset of the right panel of Fig. 2. The sample is loaded in the hole of gasket and surrounded by adiabatic and insulating pressure medium c-BN. When there is external heating, the temperature gradient between

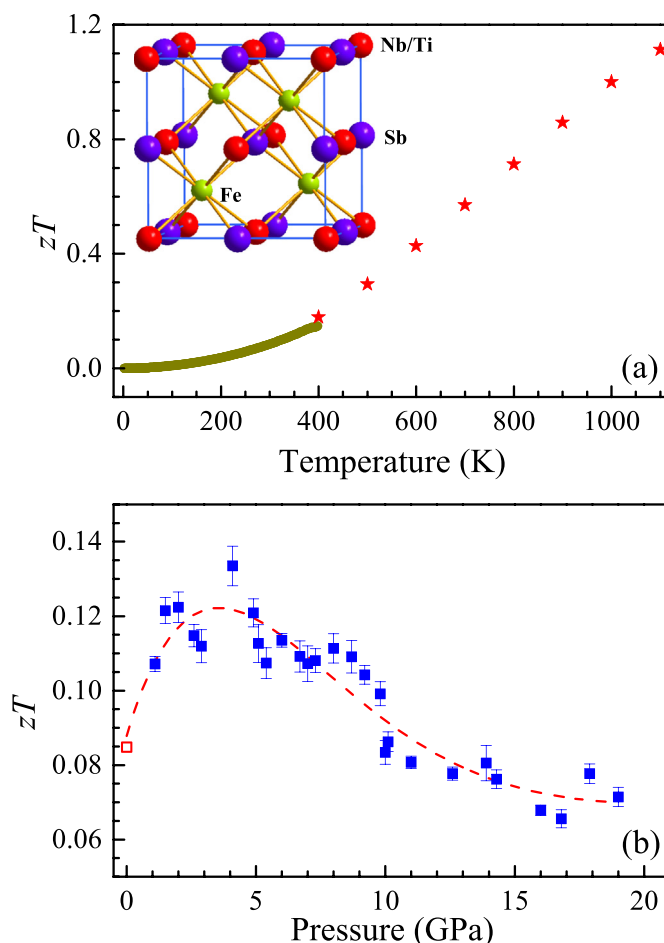
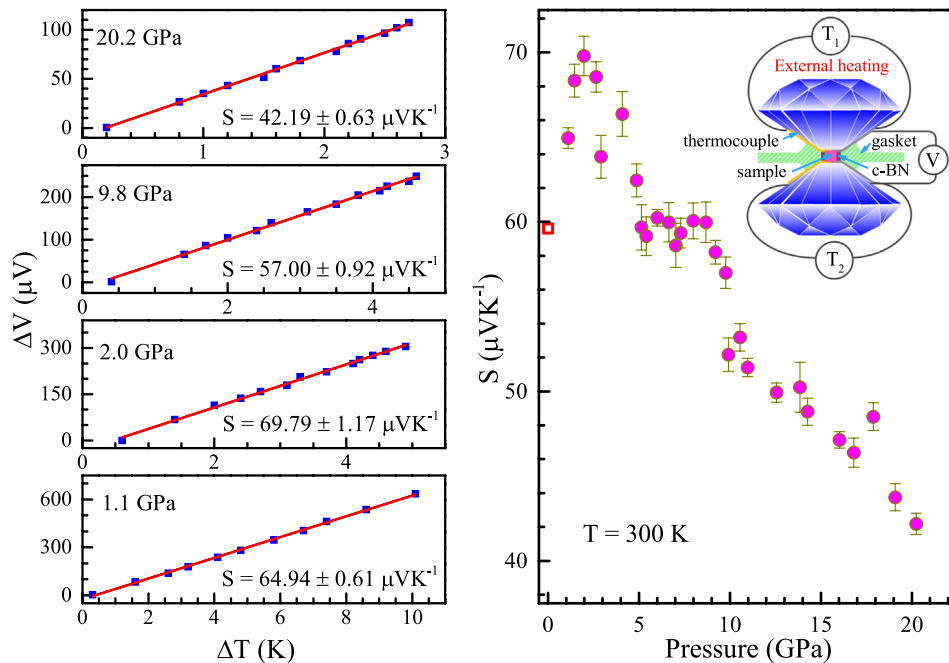


Fig. 1. (a) Temperature dependence of the dimensionless figure of merit  $zT$  for  $\text{FeNb}_{0.8}\text{Ti}_{0.2}\text{Sb}$  at ambient pressure. The inset is the crystal structure of the sample. (b) Pressure dependence of  $zT$  for  $\text{FeNb}_{0.8}\text{Ti}_{0.2}\text{Sb}$  around room temperature. The red dotted line represents the guide to the eye. (For interpretation of the references to colour in this figure legend, the reader is referred to the Web version of this article.)

the hot side and the cold side will be measured by the K-type thermocouples. Meanwhile, the thermoelectric voltage will be collected by a digital nanovoltmeter (218-A-5900, Keithley) [14,15]. The right panel of Fig. 2 presents the pressure dependence of Seebeck coefficient for  $\text{FeNb}_{0.8}\text{Ti}_{0.2}\text{Sb}$  at 300 K. The red square represents the ambient pressure data. As can be seen, the Seebeck coefficient increases sharply with increasing pressure, exhibiting a pronounced maximum around 2 GPa. Then with the increasing pressure, the Seebeck coefficient decreases rapidly.

The representative temperature dependent resistivity at the selected pressure are demonstrated in Fig. 3(a). The resistivity of  $\text{FeNb}_{0.8}\text{Ti}_{0.2}\text{Sb}$  under pressure was measured by four-probe method. The four Pt electrodes are symmetrically located on the sample as shown in the inset of Fig. 3(a). As observed, the temperature-dependent resistivity is gradually suppressed with increasing pressure. However, an anomaly is found above 10 GPa. The suppression of pressure on resistivity disappears. And then, the resistivity increases with increasing pressure. The corresponding electrical conductivity as a function of pressure are plotted in Fig. 3(b). An increase in electrical conductivity before 4 GPa is observed. The electrical conductivity also exhibits the weak anomaly near 4 GPa. The curve shows a plateau between 4 and 10 GPa and then decreases at higher pressures.

At present, there is no complete understanding on how pressure



**Fig. 2.** Left: The representative relationship between the thermoelectric voltage ( $\Delta V$ ) and  $\Delta T$  at the selected pressures of 1.1, 2.0, 9.8 and 20.2 GPa. Right: Pressure dependence of the Seebeck coefficient for  $\text{FeNb}_{0.8}\text{Ti}_{0.2}\text{Sb}$  around room temperature. The inset of the right panel illustrates the diagram of the Seebeck coefficient measurement under pressure.

changes the band structure of  $\text{FeNb}_{0.8}\text{Ti}_{0.2}\text{Sb}$ . Electronic band calculations show that the valence band maximum of  $\text{FeNbSb}$  locates at the  $L$  point with twofold orbital degeneracy. The band gap of  $\text{FeNbSb}$  is about 0.54 eV [18,38]. The band effective mass of  $\text{FeNbSb}$  is  $1.6 m_e$ . Substituting Ti at Nb site has been proved to have no effect on the valence band structure, because the valence band structure is dominated by the electronic character of the Fe element [33]. The decrease in band effective mass is beneficial for the increase of carrier mobility ( $\mu$ ). Since pressure application leads to narrowing of the forbidden gap, and therefore, to the increase in the carrier concentration ( $n$ ), it eventually brings to the intrinsic conductivity.

As a degenerate semiconductor, the Seebeck coefficient of  $\text{FeNb}_{0.8}\text{Ti}_{0.2}\text{Sb}$  can be approximated by the Mott formula [4]:

$$S = \frac{\pi^2 k_B^2 T}{3e} \left\{ \frac{1}{n} \frac{dn(E)}{dE} + \frac{1}{\mu} \frac{d\mu(E)}{dE} \right\}_{E=E_F}, \quad (1)$$

The Seebeck coefficient will be beneficial from the enhanced energy dependence of the carrier concentration and carrier mobility. The formula reveals that there are two mechanisms that can increase the Seebeck coefficient. One is an increased energy-dependent of carrier concentration, for instance by a local increase in the density of states. The other is an increased energy-dependent of carrier mobility, for instance by a scattering mechanism that strongly depends on the energy of the charge carriers. The electrical conductivity is also related to carrier concentration and carrier mobility through  $\sigma = ne\mu$ .

In order to understand the origin of such phenomena in the electrical transport properties, we investigate the carrier concentration and carrier mobility under pressure by Hall effect measurement. The representative Hall resistivity as a function of magnetic field measured at room temperature are shown at the left panel of Fig. 4. The Hall resistivity varies with the applied field in a linear behavior. We thus perform linear fitting to the data. The slope of the curve gives the Hall coefficient ( $R_H$ ). Then, the carrier concentration is calculated through the formula  $n_H = 1/eR_H$ , where  $e$  is the unit of the charge. Accordingly, the carrier mobility is

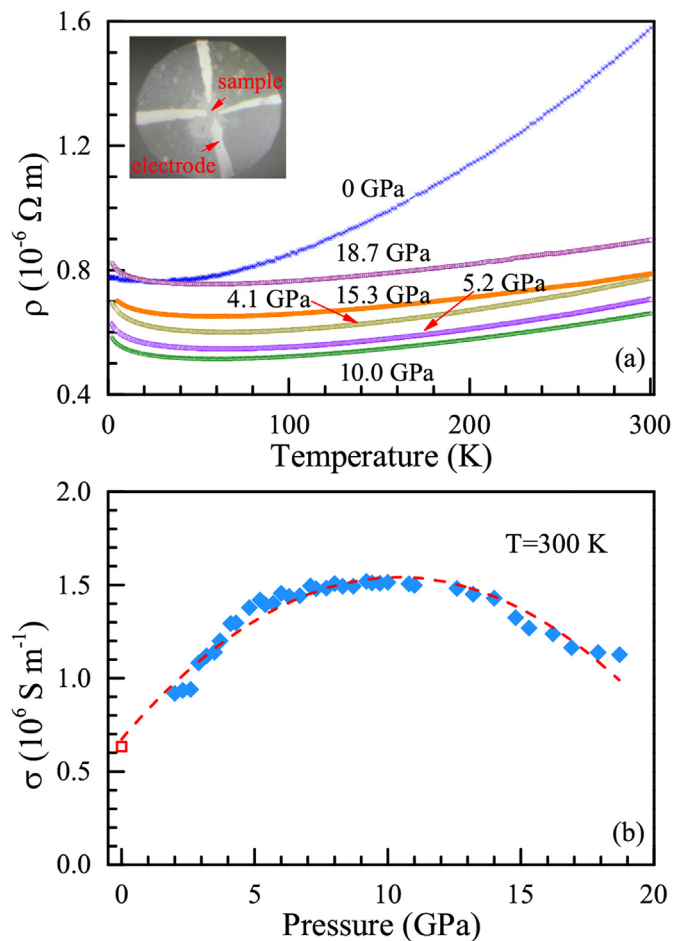


**Fig. 3.** (a) The representative temperature dependence of the resistivity at the selected pressures. The inset shows the geometry of the four electrodes. (b) Pressure dependence of the electrical conductivity of  $\text{FeNb}_{0.8}\text{Ti}_{0.2}\text{Sb}$  around room temperature.

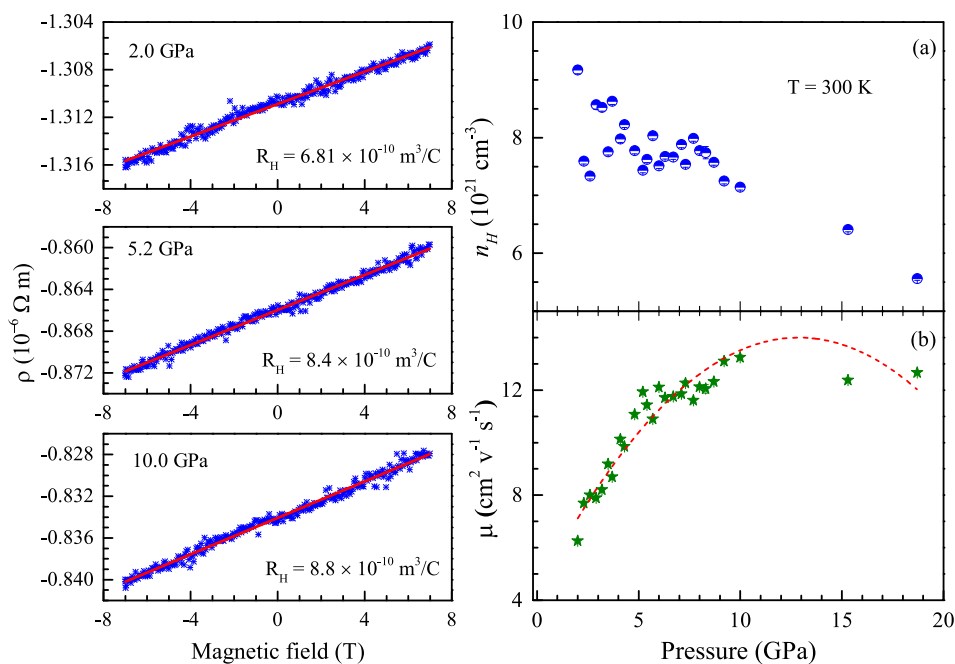


**Fig. 4.** Left: Magnetic field dependence of the Hall resistivity measured at room temperature at the selected pressures. Right: Pressure dependence of the carrier concentration (a) and carrier mobility (b) of  $\text{FeNb}_{0.8}\text{Ti}_{0.2}\text{Sb}$  at room temperature.

obtained. The pressure dependent carrier concentration and carrier mobility are presented in Fig. 4(a) and (b), respectively. The carrier concentration with the optimal value of  $10^{21} \text{ cm}^{-3}$  exhibits a small increase before 5 GPa and then declines rapidly with increasing pressure. A corresponding change in carrier mobility occurs. The carrier mobility as a function of pressure are plotted in Fig. 4(b). The carrier mobility increases with pressure. The curve shows a plateau between 10 and 15 GPa and then decreases at higher pressures. The

results are in accordance with the Seebeck coefficient and electrical conductivity. Therefore, the enhanced Seebeck coefficient is beneficial from the increased carrier mobility at low pressures.

From the high-pressure X-ray diffraction and Raman scattering measurements, no structural phase transition has been found in  $\text{FeNb}_{0.8}\text{Ti}_{0.2}\text{Sb}$  up to at least 42 GPa [36]. Therefore, the asymmetrical form of Seebeck coefficient and the anomaly in the electrical conductivity are not caused by structural phase transition. We

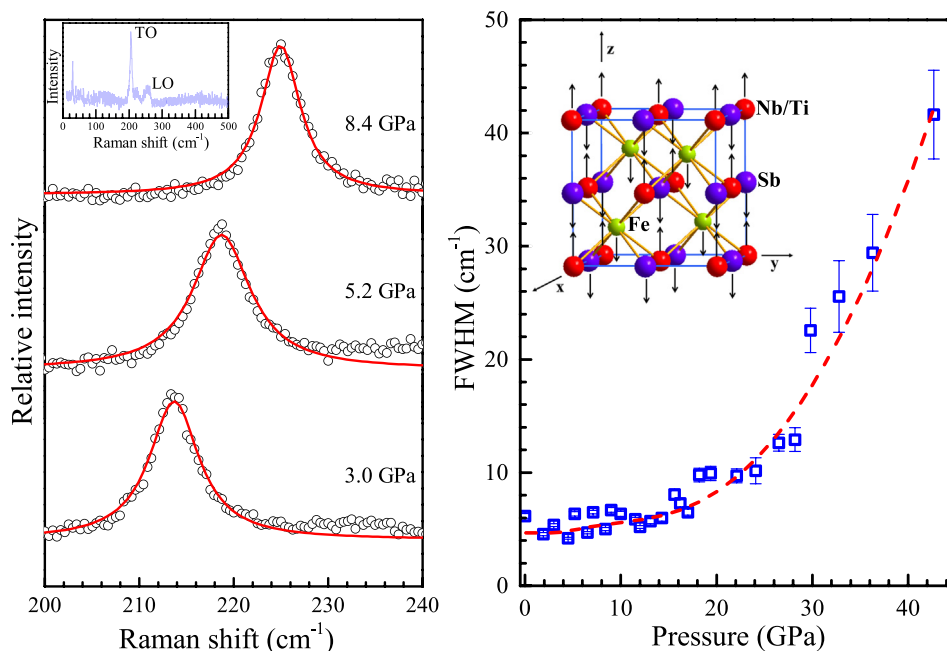


**Fig. 5.** (Color online) Left: The representative Raman spectra of the TO mode at different pressures. Right: The pressure dependence of the FWHM obtained from Lorentz fitting to the data. The inset of the left panel shows the Raman spectrum of  $\text{FeNb}_{0.8}\text{Ti}_{0.2}\text{Sb}$  at ambient condition. The inset of the right panel presents the assignment for the TO mode in a  $\text{FeNb}_{0.8}\text{Ti}_{0.2}\text{Sb}$  unit cell. The arrows represent the vibrational directions of the atoms, green for Fe, red for Nb/Ti, purple for Sb. (For interpretation of the references to colour in this figure legend, the reader is referred to the Web version of this article.)

assign the behavior to the pressure-driven electron topological transition (ETT) [39]. The signature of ETT is that the application of external influence on a material causes a reshaping of the Fermi surface of the material without changing the physical structure of the crystal. Specifically, the thermoelectric phenomena in thermoelectric materials could provide information for an ETT [40]. In the vicinity of ETT, the Seebeck coefficient and electrical conductivity will be abnormal. For example, an asymmetric maximum in the Seebeck coefficient will occur [41]. The Hall coefficient will reflect the change of Fermi surface and provide evidence for the occurrence of the ETT. Accordingly, the anomalies in the Seebeck coefficient and electrical conductivity for  $\text{FeNb}_{0.8}\text{Ti}_{0.2}\text{Sb}$  meet the conditions of ETT. Therefore, the ETT leads to these anomalies of electrical transport properties in the sample.

The pressure-dependent thermal conductivity was estimated through the full width at half-maximum (FWHM) of phonon peak. Due to the limitations of the high-pressure thermal transport property measurement, the measurement of thermal conductivity under pressure remains a challenge. The total thermal conductivity includes lattice thermal conductivity ( $\kappa_l$ ) and electronic thermal conductivity ( $\kappa_e$ ). The lattice thermal conductivity is usually determined by the phonon transport behavior in crystals. In the relaxation time approximation, the lattice thermal conductivity for phonons of wave vector  $q$  and branch  $j$  is given by Ref. [42]:

$$\kappa_{qj} = \frac{1}{3} C_{qj} v_{qj} \lambda_{qj} = \frac{1}{3} C_{qj} v_{qj}^2 \tau_{qj}, \quad (2)$$

where  $C_{qj}$  is the phonon heat capacity and  $v_{qj} = \frac{\partial E_{qj}}{\partial q}$  is the group velocity determined by local dispersion gradients. The phonon mean free paths  $\lambda_{qj} = v_{qj} \tau_{qj}$  depend on the measured full width at half-maximum (FWHM) of phonon peak through the relaxation time [43]  $\tau_{qj} = \frac{1}{2\pi \text{FWHM}_{qj}}$ .

Phonon spectrum could provide information of phonon vibration and will be helpful to understand the lattice thermal conductivity. The Raman spectrum for  $\text{FeNb}_{0.8}\text{Ti}_{0.2}\text{Sb}$  with two phonon modes at ambient condition is illustrated in the inset of the left panel of Fig. 5. Due to the high intensity, the TO mode is chosen for the investigation. The TO mode is the motions of Nb/Ti against both counter atoms (Fe and Sb). The representative Raman spectra of the TO mode at different pressures are shown at the left panel of Fig. 5. In order to obtain the evolution of phonon peak with pressure, the data were analyzed by Lorentz fitting. The pressure dependent FWHM of the TO mode is presented at the right panel of Fig. 5. As can be seen, the FWHM of the TO mode is nearly a constant below 4 GPa. The behavior is likely important to the thermal transport. The lattice thermal conductivity of  $\text{FeNb}_{0.8}\text{Ti}_{0.2}\text{Sb}$  may not increase much under pressure. The result would be beneficial for the increased  $zT$ .

Previous study has found that the lattice thermal conductivity and FWHM of the phonon peak is a constant [44]. Therefore, if we know the constant and the FWHM of the phonon peak, the lattice thermal conductivity could be obtained. Fortunately, the constant for  $\text{FeNb}_{0.8}\text{Ti}_{0.2}\text{Sb}$  can be obtained from the lattice thermal conductivity and FWHM at ambient pressure through  $A = \kappa_l \text{FWHM}$ , where  $A$  is the constant. The value of the constant for  $\text{FeNb}_{0.8}\text{Ti}_{0.2}\text{Sb}$  is  $0.2 \text{ WK}^{-1} \text{m}^{-2}$ . As a consequence, the rough guess and estimation of the lattice thermal conductivity under pressure can be obtained through  $\kappa_l = A \text{FWHM}$ , as shown in Fig. 6(a).

The electronic thermal conductivity is related to the electrical conductivity via the Wiedemann-Franz Law:  $\kappa_e = L\sigma T$ , where  $L$  is the Lorenz number and can be calculated using the single parabolic band (SPB) model with reasonable approximation [35]. In an estimation of the electronic thermal conductivity of  $\text{FeNb}_{0.8}\text{Ti}_{0.2}\text{Sb}$

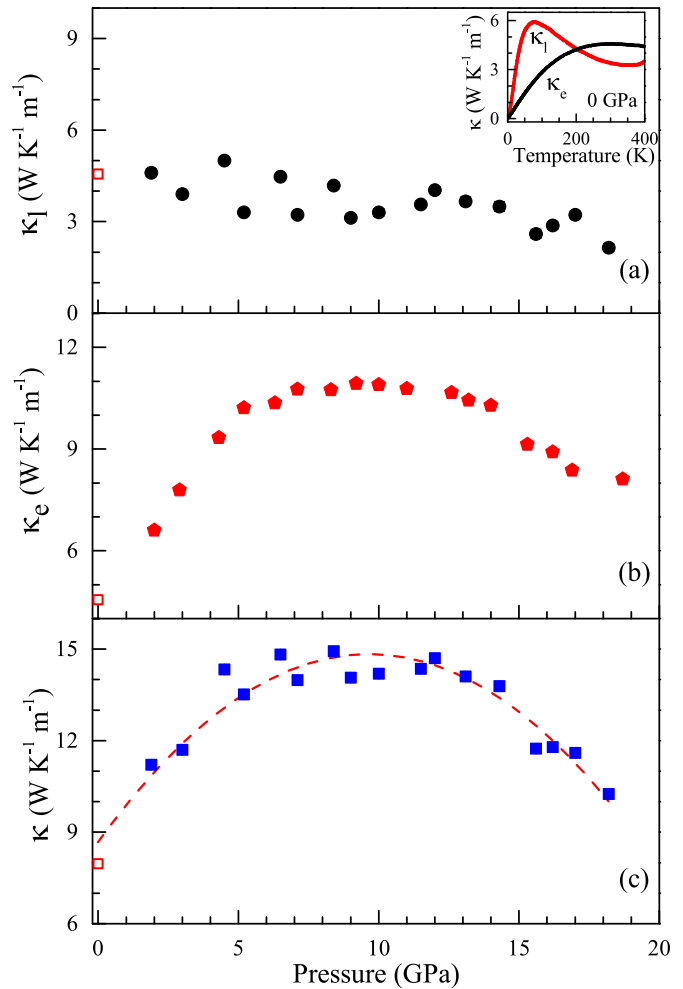


**Fig. 6.** Pressure dependence of the lattice thermal conductivity (a), electronic thermal conductivity (b) and thermal conductivity of  $\text{FeNb}_{0.8}\text{Ti}_{0.2}\text{Sb}$  around room temperature. The inset of (a): Temperature dependence of electronic and lattice thermal conductivity for  $\text{FeNb}_{0.8}\text{Ti}_{0.2}\text{Sb}$  at ambient pressure.

under pressure, we assume that the Lorenz number is a constant. The corresponding data are shown in Fig. 6(b). As a result, a rough estimation of the total thermal conductivity as a function of pressure is obtained, shown in Fig. 6(c). In a recent experimental study [34], we found that electrons contribute more than lattice to the thermal conductivity above 200 K, as shown in the inset of Fig. 6(a). The thermal conductivity is obviously governed by electronic transports at ambient temperature. At high pressures, the electronic component still dominates the thermal conductivity.

Pressure tuning is a method to change the physical properties through lattice shrinking. Compared with the temperature-tuning effect on thermoelectric performance, pressure tuning is more flexible and convenient. Although our measurements report an estimation of the thermal conductivity, a qualitative understanding of the thermal transport property under pressure is valuable for the thermoelectric material research. By means of pressure, the Seebeck coefficient and electrical conductivity are obviously enhanced. The  $zT$  value of room-temperature  $\text{FeNb}_{0.8}\text{Ti}_{0.2}\text{Sb}$  exhibits a moderate increase with pressure. Previous reports show that the high-pressure  $zT$  values of  $\text{CuInTe}_2$  [14] and palladium sulfide [15] are enhanced by about 5 times and 6 times, respectively. Especially, the carrier concentration of  $\text{CuInTe}_2$  and palladium sulfide are largely improved to the optimal range under pressure. Therefore, the

reason for the relatively low increase in  $\text{FeNb}_{0.8}\text{Ti}_{0.2}\text{Sb}$  is that the carrier concentration has already been optimized from doping and will not change much under pressure. Compared with the state of the art near-room-temperature thermoelectric materials, such as  $\text{Bi}_2\text{Te}_3$ -based alloys [45], the  $zT$  value of room-temperature  $\text{FeNb}_{0.8}\text{Ti}_{0.2}\text{Sb}$  under pressure is still relatively low. However, the increase in  $zT$  under pressure is promising and thus provides the guidance for the half-Heusler materials with higher starting  $zT$  values.

#### 4. Conclusions

In summary, we have performed a series of measurements of pressure dependent Seebeck coefficient, electrical conductivity, and thermal conductivity on an efficient thermoelectric half-Heusler material at room temperature. The results demonstrate that a further enhancement can still be realized in a highly efficient thermoelectric half-Heusler  $\text{FeNb}_{0.8}\text{Ti}_{0.2}\text{Sb}$ , which holds the high  $zT$  value in the half-Heusler family. The rapid increase in Seebeck coefficient and the steady increase in the electrical conductivity together dominate the improvement of the thermoelectric performance. Such an improvement is proposed to be driven by the pressure-induced ETT. In addition, the results provide guidance to proceed the research for high conversion efficiency thermoelectric materials.

#### Acknowledgements

The sample preparation was supported by the National Natural Science Foundation of China (No. 11574267).

#### References

- J.F. Li, W.S. Liu, L.D. Zhao, M. Zhou, High-performance nanostructured thermoelectric materials, *NPG Asia Mater.* 2 (2010) 152–158, <https://doi.org/10.1038/asiamat.2010.138>.
- X. Shi, L.D. Chen, C. Uher, Recent advances in high-performance bulk thermoelectric materials, *Int. Mater. Rev.* 61 (2016) 379–415, <https://doi.org/10.1080/09506608.2016.1183075>.
- Z.F. Ren, Y.C. Lan, Q.Y. Zhang, *Advanced Thermoelectrics: Materials, Contacts, Devices, and Systems*, CRC Press, 2017.
- T.J. Zhu, Y.T. Liu, C.G. Fu, J.P. Heremans, J.G. Snyder, X.B. Zhao, Compromise and synergy in high-efficiency thermoelectric materials, *Adv. Mater.* 29 (2017) 1605884, <https://doi.org/10.1002/adma.201605884>.
- G.J. Snyder, E.S. Toberer, Complex thermoelectric materials, *Nat. Mater.* 7 (2008) 105–114, <https://doi.org/10.1038/nmat2090>.
- X. Shi, J. Yang, J.R. Salvador, M.F. Chi, J.Y. Cho, H. Wang, S.Q. Bai, J.H. Yang, W.Q. Zhang, L.D. Chen, Multiple-filled skutterudites: high thermoelectric figure of merit through separately optimizing electrical and thermal transports, *J. Am. Chem. Soc.* 133 (2011) 7837–7846, <https://doi.org/10.1021/ja111199y>.
- H.Z. Zhao, J.E. Sui, Z.J. Tang, Y.C. Lan, Q.G. Jie, D. Kraemer, K.N. McEnaney, A. Guloy, G. Chen, Z.F. Ren, High thermoelectric performance of  $\text{MgAgSb}$ -based materials, *Nano Energy* 7 (2014) 97–103, <https://doi.org/10.1016/j.nanoen.2014.04.012>.
- C.G. Fu, S.Q. Bai, Y.T. Liu, Y.S. Tang, L.D. Chen, X.B. Zhao, T.J. Zhu, Realizing high figure of merit in heavy-band  $p$ -type half-Heusler thermoelectric materials, *Nat. Commun.* 6 (2015) 8144, <https://doi.org/10.1038/ncomms9144>.
- Y. He, P. Lu, X. Shi, F.F. Xu, T.S. Zhang, G.J. Snyder, C. Uher, L.D. Zhao, Ultrahigh thermoelectric performance in mosaic crystals, *Adv. Mater.* 27 (2015) 3639–3644, <https://doi.org/10.1002/adma.201501030>.
- J. Shuai, H.Y. Geng, Y.C. Lan, Z. Zhu, C. Wang, Z.H. Liu, J.M. Bao, C.W. Chu, J.H. Sui, Z.F. Ren, Higher thermoelectric performance of Zintl phases  $(\text{Eu}^{0.5}\text{Yb}^{0.5})_{1-x}\text{Ca}_x\text{Mg}_2\text{Bi}_2$  by band engineering and strain fluctuation, *Proc. Natl. Acad. Sci.* 113 (2016) E4125–E4132, <https://doi.org/10.1073/pnas.1608794113>.
- Y.Z. Pei, J. Lesh-Falk, E.S. Toberer, D.L. Medlin, G.J. Snyder, High thermoelectric performance in  $\text{pBtTe}$  due to large nanoscale  $\text{Ag}_2\text{Te}$  precipitates and  $\text{La}$  doping, *Adv. Funct. Mater.* 21 (2011) 241–249, <https://doi.org/10.1002/adfm.201000878>.
- G. Joshi, H. Lee, Y.C. Lan, X.W. Wang, G.H. Zhu, D.Z. Wang, R.W. Gould, D.C. Cuff, M.Y. Tang, M.S. Dresselhaus, G. Chen, Z.F. Ren, Enhanced thermoelectric figure-of-merit in nanostructured  $p$ -type silicon germanium bulk alloys, *Nano Lett.* 8 (2008) 4670–4674, <https://doi.org/10.1021/nl8026795>.
- K. Biswas, J. He, I.D. Blum, C.I. Wu, T.P. Hogan, D.N. Seidman, V.P. Draid, M.G. Kanatzidis, High-performance bulk thermoelectrics with all-scale hierarchical architectures, *Nature* 489 (2012) 414–418, <https://doi.org/10.1038/nature11439>.
- H. Yu, L.C. Chen, H.J. Pang, X.Y. Qin, P.F. Qiu, X. Shi, L.D. Chen, X.J. Chen, Large enhancement of thermoelectric performance in  $\text{CuInTe}_2$  upon compression, *Mater. Today Phys.* 5 (2018) 1–6, <https://doi.org/10.1016/j.mtphys.2018.04.002>.
- L.C. Chen, H. Yu, H.J. Pang, B.B. Jiang, L. Su, X. Shi, L.D. Chen, X.J. Chen, Pressure-induced enhancement of thermoelectric performance in palladium sulfide, *Mater. Today Phys.* 5 (2018) 64–71, <https://doi.org/10.1016/j.mtphys.2018.05.004>.
- J.F. Meng, N.V.C. Shekar, J.V. Badding, Threefold enhancement of the thermoelectric figure of merit for pressure tuned  $\text{Sr}_8\text{Ga}_{16}\text{Ge}_{30}$ , *J. Appl. Phys.* 89 (2001) 1730–1733, <https://doi.org/10.1063/1.1334366>.
- S.V. Ovsyannikov, V.V. Shchennikov, G.V. Vorontsov, A.Y. Manakov, A.Y. Likhacheva, V.A. Kulbachinskii, Giant improvement of thermoelectric power factor of  $\text{Bi}_2\text{Te}_3$  under pressure, *J. Appl. Phys.* 104 (2008), 053713, <https://doi.org/10.1063/1.2973201>.
- D.P. Young, P. Khalifah, R.J. Cava, Thermoelectric properties of pure and doped  $\text{FeMsb}$  ( $M=\text{V}, \text{Nb}$ ), *J. Appl. Phys.* 87 (2000) 317–321, <https://doi.org/10.1063/1.371863>.
- J. Yang, H. Li, T. Wu, W.Q. Zhang, L.D. Chen, J.H. Yang, Evaluation of half-Heusler compounds as thermoelectric materials based on the calculated electrical transport properties, *Adv. Funct. Mater.* 18 (2008) 2880–2888, <https://doi.org/10.1002/adfm.200701369>.
- S. Populoh, M.H. Aguirre, O.C. Brunko, K. Galazka, Y. Lu, A. Weidenkaff, High figure of merit in (Ti, Zr, Hf) half-Heusler alloys, *Scr. Mater.* 66 (2012) 1073–1076, <https://doi.org/10.1016/j.scriptamat.2012.03.002>.
- S. Chen, Z.F. Ren, Recent progress of half-Heusler for moderate temperature thermoelectric applications, *Mater. Today* 16 (2013) 387–395, <https://doi.org/10.1016/j.mattod.2013.09.015>.
- S. Chen, K.C. Lukas, W.S. Liu, C.P. Opeil, G. Chen, Z.F. Ren, Effect of hf concentration on thermoelectric properties of nanostructured  $n$ -type half-Heusler materials  $\text{Hf}_x\text{Zr}_{1-x}\text{NiSn}_{0.99}\text{Sb}_{0.01}$ , *Adv. Energy Mater.* 3 (2013) 1210–1214, <https://doi.org/10.1002/aenm.201300336>.
- T.J. Zhu, C.G. Fu, H.H. Xie, Y.T. Liu, X.B. Zhao, High efficiency half-Heusler thermoelectric materials for energy harvesting, *Adv. Energy Mater.* 5 (2015) 1500588, <https://doi.org/10.1002/aenm.201500588>.
- R. He, D. Kraemer, J. Mao, L.P. Zeng, Q. Jie, Y.C. Lan, C.H. Li, J. Shuai, H.S. Kim, Y. Liu, D. Broido, C.W. Chu, G. Chen, Z.F. Ren, Achieving high power factor and output power density in  $p$ -type half-Heuslers  $\text{Nb}_{1-x}\text{Ti}_x\text{FeSb}$ , *Proc. Natl. Acad. Sci. U. S. A.* 113 (2016) 13576–13581, <https://doi.org/10.1073/pnas.1617663113>.
- R. He, H.T. Zhu, J.Y. Sun, J. Mao, H. Reith, S. Chen, G. Schiernin, K. Nielsch, Z.F. Ren, Improved thermoelectric performance of  $n$ -type half-Heusler  $\text{MCo}_{1-x}\text{Ni}_x\text{Sb}$  ( $M = \text{Hf}, \text{Zr}$ ), *Mater. Today Phys.* 1 (2017) 24–30, <https://doi.org/10.1016/j.mtphys.2017.05.002>.
- G. Joshi, R. He, M. Engber, G. Samsonidze, T. Pantha, E. Dahal, K. Dahal, J. Yang, Y.C. Lan, B. Kozinsky, Z.F. Ren, Nbfesb-based  $p$ -type half-Heuslers for power generation applications, *Energy Environ. Sci.* 7 (2014) 4070–4076, <https://doi.org/10.1039/C4EE02180K>.
- C.G. Fu, T.J. Zhu, Y.Z. Pei, H.H. Xie, H. Wang, G.J. Snyder, High band degeneracy contributes to high thermoelectric performance in  $p$ -type half-Heusler compounds, *Adv. Energy Mater.* 4 (2014) 1400600, <https://doi.org/10.1002/aenm.201400600>.
- J.J. Shen, C.G. Fu, Y.T. Liu, X.B. Zhao, T.J. Zhu, Enhancing thermoelectric performance of  $\text{FeNbSb}$  half-Heusler compound by Hf-Ti dual-doping, *Energy Storage Mater.* 10 (2018) 69–74, <https://doi.org/10.1016/j.ensm.2017.07.014>.
- G. Joshi, X. Yan, H.Z. Wang, W.S. Liu, G. Chen, Z.F. Ren, Enhancement in the thermoelectric figure of merit of an  $p$ -type half-Heusler compound by the nanocomposite approach, *Adv. Energy Mater.* 1 (2011) 643–647, <https://doi.org/10.1002/aenm.201100126>.
- X. Yan, W.S. Liu, H. Wang, S. Chen, J. Shiomi, K. Esfarjani, H.Z. Wang, D.Z. Wang, G. Chen, Z.F. Ren, Stronger phonon scattering by larger differences in atomic mass and size in  $p$ -type half-Heuslers  $\text{Hf}_{1-x}\text{Ti}_x\text{CoSb}_{0.8}\text{Sn}_{0.2}$ , *Energy Environ. Sci.* 5 (2012) 7543–7548, <https://doi.org/10.1039/C2EE21554C>.
- Y.T. Liu, H.H. Xie, C.G. Fu, G.J. Snyder, X.B. Zhao, T.J. Zhu, Demonstration of a phonon-glass electron-crystal strategy in (Hf,Zr)NiSn half-Heusler thermoelectric materials by alloying, *J. Mater. Chem.* 3 (2015) 22716–22722, <https://doi.org/10.1039/C5TA04418A>.
- Y.T. Liu, C.G. Fu, K.Y. Xia, J.J. Yu, X.B. Zhao, H.G. Pan, C. Felser, T.J. Zhu, Lanthanide contraction as a design factor for high performance half-Heusler thermoelectric materials, *Adv. Mater.* 30 (2018) 1800881–1800887, <https://doi.org/10.1002/adma.201800881>.
- C.G. Fu, T.J. Zhu, Y.T. Liu, H.H. Xie, X.B. Zhao, Band engineering of high performance  $p$ -type  $\text{FeNbSb}$  based half-Heusler thermoelectric materials for figure of merit  $zT >$ , *Energy Environ. Sci.* 8 (2015) 216–220, <https://doi.org/10.1039/C4EE03042G>.
- H.J. Pang, C.G. Fu, H. Yu, L.C. Chen, T.J. Zhu, X.J. Chen, Origin of efficient thermoelectric performance in half-Heusler  $\text{FeNb}_{0.8}\text{Ti}_{0.2}\text{Sb}$ , *J. Appl. Phys.* 123 (2018) 235106, <https://doi.org/10.1063/1.5030938>.
- H.H. Xie, H. Wang, Y.Z. Pei, C.G. Fu, X.H. Liu, G.J. Snyder, X.B. Zhao, T.J. Zhu, Beneficial contribution of alloy disorder to electron and phonon transport in half-Heusler thermoelectric materials, *Adv. Funct. Mater.* 23 (2013) 5123–5130, <https://doi.org/10.1002/adfm.201300663>.

- [36] H.J. Pang, L.C. Chen, Z.Y. Cao, Y. Hao, C.G. Fu, T.J. Zhu, A.F. Goncharov, X.J. Chen, Mode gruneisen parameters of an efficient thermoelectric half-heusler, *J. Appl. Phys.* 124 (2018) 195107, <https://doi.org/10.1063/1.5050697>.
- [37] H.K. Mao, P.M. Bell, J.W. Shaner, D.J. Stembey, Specific volume measurements of Cu, Mo, Pd, and Ag and calibration of the ruby R1 fluorescence pressure gauge from 0.06 to 1 Mbar, *J. Appl. Phys.* 24 (1963) 118–173, <https://doi.org/10.1063/1.325277>.
- [38] L. Jodin, J. Tobola, P. Pecher, H. Scherrer, S. Kaprzyk, Effect of substitutions and defects in half-heusler FeVSb studied by electron transport measurements and kkr-cpa electronic structure calculations, *Phys. Rev. B* 70 (2004) 184207, <https://doi.org/10.1103/PhysRevB.70.184207>.
- [39] I.M. Lifshitz, Anomalies of electron characteristics of a metal in the high pressure region, *Sov. Phys. - JETP* 11 (1960) 1130–1135, [https://doi.org/10.1016/0003-4916\(63\)90068-X](https://doi.org/10.1016/0003-4916(63)90068-X).
- [40] A.A. Abrikosov, Fundamentals of the theory of metals, *Phys. Today* 43 (1990) 73–76, <https://doi.org/10.1063/1.2810530>.
- [41] Y.M. Blanter, M.I. Kaganov, A.V. Pantsulaya, A.A. Varlamov, The theory of electronic topological transitions, *Phys. Rep.* 245 (1994) 159–257, [https://doi.org/10.1016/0370-1573\(94\)90103-1](https://doi.org/10.1016/0370-1573(94)90103-1).
- [42] A.A. Maradudin, A.E. Fein, Scattering of neutrons by an anharmonic crystal, *Phys. Rev.* 128 (1962) 2589–2608, <https://doi.org/10.1103/PhysRev.128.2589>.
- [43] A.M. Hofmeister, Pressure dependence of thermal transport properties, *Proc. Natl. Acad. Sci. U. S. A.* 104 (2007) 9192–9197, <https://doi.org/10.1073/pnas.0610734104>.
- [44] T.R. Kakuda, A.M. Limarga, T.D. Bennett, D.R. Clarke, Evolution of thermal properties of EB-PVD 7YSZ thermal barrier coatings with thermal cycling, *Acta Mater.* 57 (2009) 2583–2591, <https://doi.org/10.1016/j.actamat.2009.02.019>.
- [45] B. Poudel, Q. Hao, Y. Ma, Y.C. Lan, A. Minnich, B. Yu, X.A. Yan, D.Z. Wang, A. Muto, D. Vashaee, X.Y. Chen, J.M. Liu, M.S. Dresselhaus, G. Chen, Z.F. Ren, High-thermoelectric performance of nanostructured bismuth antimony telluride bulk alloys, *Science* 320 (2008) 634–638, <https://doi.org/10.1126/science.1156446>.